Cerebral glutamine metabolism under hyperammonemia determined in vivo by localized 1H and 15N NMR spectroscopy

Cudalbu, Cristina; Lanz, Bernard; Duarte, João MN; Morgenthaler, Florence D; Pilloud, Yves; Mlynárik, Vladimir; Gruetter, Rolf

How to cite

CUDALBU, Cristina et al. Cerebral glutamine metabolism under hyperammonemia determined in vivo by localized 1H and 15N NMR spectroscopy. In: Journal of cerebral blood flow and metabolism, 2012, vol. 32, n° 4, p. 696–708. doi: 10.1038/jcbfm.2011.173

This publication URL: https://archive-ouverte.unige.ch/unige:33018
Publication DOI: 10.1038/jcbfm.2011.173

Journal of Cerebral Blood Flow & Metabolism (2012) 32, 696–708

www.jcbfm.com

Cerebral glutamine metabolism under hyperammonemia determined *in vivo* by localized ^{1}H and ^{15}N NMR spectroscopy

Cristina Cudalbu[1], Bernard Lanz[1], João MN Duarte[1,2], Florence D Morgenthaler[1], Yves Pilloud[1], Vladimir Mlynárik[1] and Rolf Gruetter[1,3,4]

[1]*Laboratory for Functional and Metabolic Imaging (LIFMET), Center for Biomedical Imaging (CIBM), Ecole Polytechnique Fédérale de Lausanne (EPFL), Lausanne, Switzerland;* [2]*Faculty of Biology and Medicine, University of Lausanne, Lausanne, Switzerland;* [3]*Department of Radiology, University of Lausanne, Lausanne, Switzerland;* [4]*Department of Radiology, University of Geneva, Geneva, Switzerland*

Brain glutamine synthetase (GS) is an integral part of the glutamate–glutamine cycle and occurs in the glial compartment. *In vivo* Magnetic Resonance Spectroscopy (MRS) allows noninvasive measurements of the concentrations and synthesis rates of metabolites. ^{15}N MRS is an alternative approach to ^{13}C MRS. Incorporation of labeled ^{15}N from ammonia in cerebral glutamine allows to measure several metabolic reactions related to nitrogen metabolism, including the glutamate–glutamine cycle. To measure ^{15}N incorporation into the position 5N of glutamine and position 2N of glutamate and glutamine, we developed a novel ^{15}N pulse sequence to simultaneously detect, for the first time, [5-^{15}N]Gln and [2-^{15}N]Gln + Glu *in vivo* in the rat brain. In addition, we also measured for the first time in the same experiment localized ^{1}H spectra for a direct measurement of the net glutamine accumulation. Mathematical modeling of ^{1}H and ^{15}N MRS data allowed to reduce the number of assumptions and provided reliable determination of GS (0.30 ± 0.050 μmol/g per minute), apparent neurotransmission (0.26 ± 0.030 μmol/g per minute), glutamate dehydrogenase (0.029 ± 0.002 μmol/g per minute), and net glutamine accumulation (0.033 ± 0.001 μmol/g per minute). These results showed an increase of GS and net glutamine accumulation under hyperammonemia, supporting the concept of their implication in cerebral ammonia detoxification.
Journal of Cerebral Blood Flow & Metabolism (2012) **32,** 696–708; doi:10.1038/jcbfm.2011.173; published online 14 December 2011

Keywords: ^{15}N and ^{1}H MRS; glutamate dehydrogenase; glutamine synthetase; hyperammonemia; net glutamine accumulation

Introduction

In brain, glutamine synthetase (GS) activity is predominantly localized in the astrocytes (Martinez-Hernandez *et al*, 1977; Norenberg and Martinez-Hernandez, 1979). It is responsible for the synthesis of glutamine (Gln) from glutamate (Glu) cleared from the synaptic cleft, thus having a major role in neurotransmission. This glutamine is then shuttled to neurons where it can be deaminated, completing the so-called glutamate–glutamine cycle (Berl *et al*, 1968; Clarke *et al*, 1970; Gruetter, 2004; McKenna, 2007; Shank and Aprison, 1981; Zwingmann and Leibfritz, 2003). In addition, in conditions of hyperammonemia, GS is used for detoxification of brain ammonia (Cooper and Plum, 1987; Kanamori *et al*, 1993; Kanamori and Ross, 1993). In this process, glutamine is accumulated in the brain, while glutamate concentration remains constant. Thus, glutamine accumulation requires *de-novo* synthesis from glucose, with involvement of both glutamate dehydrogenase (GDH) and aspartate aminotransferase (Berl *et al*, 1962; Shen *et al*, 1998).

Because brain GS is an integral part of the glutamate–glutamine cycle (Berl *et al*, 1968; Clarke *et al*, 1970; Shank and Aprison, 1981) and is also functioning as a detoxification pathway for cerebral ammonia (Cooper and Plum, 1987; Kanamori and

Correspondence: Dr C Cudalbu, Laboratory for Functional and Metabolic Imaging (LIFMET), Center for Biomedical Imaging (CIBM), Ecole Polytechnique Fédérale de Lausanne (EPFL), Station 6, CH F1 602 (Bâtiment CH), CH-1015 Lausanne, Switzerland.
E-mail: cristina.cudalbu@epfl.ch
This study was supported by Centre d'Imagerie BioMédicale (CIBM) of the UNIL, UNIGE, HUG, CHUV, EPFL; the Leenaards and Jeantet Foundations; the EU Grant No. MRTN-CT-2006-035801; and Swiss National Science Foundation (SNF Grant 131087).
Received 27 July 2011; revised 31 October 2011; accepted 10 November 2011; published online 14 December 2011

Ross, 1993; Kanamori *et al*, 1993), developments of new methods for the noninvasive measurement of the GS activity became important. Several *in vitro* studies were performed to measure the GS activity in rat brain homogenates (Butterworth *et al*, 1988) or in cultured rat and mouse brain astrocytes (Yudkoff *et al*, 1986). However, knowledge of *in vivo* GS activity is necessary because glial–neuronal interaction has a crucial role in the glutamate–glutamine cycle (Erecinska and Silver, 1990). ^{13}N-labeled ammonia has been used to study the cerebral uptake and metabolism of ammonia in conscious rat (Cooper *et al*, 1979). However, the rate of GS was not determined, because the isotope enrichment of the precursor ammonia and the physical size of the compartment were not known (Cooper *et al*, 1979; Kanamori and Ross, 1993). A potential drawback of ^{13}N is its short half-life (10 minutes) which limits its usefulness to experiments of <1 hour (Cooper *et al*, 1979). *In vivo* Magnetic Resonance Spectroscopy (MRS) is a useful technique for the continuous and noninvasive measurement of the concentrations and synthesis rates of individual metabolites within precisely defined areas in the brain. In particular, *in vivo* noninvasive ^{13}C MRS has been used to study metabolic fluxes, enzymes activities in the living brain of animals and humans (Duarte *et al*, 2011; Gruetter *et al*, 2001). ^{15}N MRS is an alternative approach to ^{13}C MRS in studying glutamate–glutamine metabolism and can in principle provide a more direct interpretation than ^{13}C studies. The wide chemical shift dispersion of ^{15}N provides resolution of important metabolites in glutamine–glutamate cycle. Sparse *in vivo* ^{15}N studies and utilization of different protocols for infusion of ^{15}N-enriched substrates lead to a diversity of results and limited their integration on mathematical models of compartmentalized brain intermediary metabolism.

From these previous studies (Kanamori *et al*, 1993, 1996; Kanamori and Ross, 1993; Shen *et al*, 1998), discrepancies have been noticed concerning the GS flux (V_{syn}) and the net glutamine accumulation (also called *de-novo* glutamine synthesis rate; Shen *et al*, 1998). These divergences could be intrinsically bound to the employment of different experimental protocols and assumptions used to calculate the metabolic fluxes. Therefore, there is a need to acquire additional experimental data during the same experiment, to minimize the number of assumptions to be done on mathematical modeling.

A few past *in vivo* MRS studies under ammonia infusion used either *in vivo* ^{1}H (Fitzpatrick *et al*, 1989) or unlocalized ^{15}N spectroscopy (Kanamori *et al*, 1993, 1996; Kanamori and Ross, 1993; Shen *et al*, 1998) but never combined and used *in vitro* brain extracts (biochemical assays or high-resolution nuclear magnetic resonance (NMR)) for absolute quantification. These studies mainly focused on the incorporation of ^{15}N of ammonia into [5-^{15}N]Gln and measured the apparent GS flux (Kanamori *et al*, 1993, 1996; Kanamori and Ross, 1993; Shen *et al*, 1998).

The incorporation of ^{15}N into [2-^{15}N]Gln + Glu may provide further insight into the net flux through GDH (V_{GDH}) (Kanamori and Ross, 1995). However, due to the large chemical shift dispersion between [5-^{15}N]Gln and [2-^{15}N]Gln + Glu, V_{syn} and V_{GDH} were never simultaneously determined. Kanamori and Ross (1995) measured [2-^{15}N]Gln + Glu (but not [5-^{15}N]Gln) during ^{15}N-enriched ammonia infusion and estimated V_{GDH}.

In this context, we used a new acquisition strategy combined with an appropriate mathematical model of compartmentalized cerebral glutamine metabolism and determined, in the same experiment, an important number of metabolic fluxes with minimal assumptions. For that purpose, we developed a new ^{15}N pulse sequence to simultaneously detect, for the first time [5-^{15}N]Gln and [2-^{15}N]Gln + Glu *in vivo*. Together with *in vivo* localized ^{15}N spectra, we additionally measured for the first time in the same experiment localized ^{1}H spectra for a direct measurement of the net glutamine accumulation. From our knowledge, the combination of localized ^{15}N MRS and ^{1}H MRS in interleaved mode has not been reported previously under ^{15}N ammonia infusion. Consequently, ^{1}H MRS allowed to follow up the total Gln accumulation during ammonia infusion and thereby to directly measure the net glutamine accumulation without any assumptions. Mathematical modeling of ^{1}H and ^{15}N MRS data provided reliable estimations of V_{syn}, the apparent neurotransmission rate V_{nt}, V_{GDH}, and the net glutamine accumulation ($V_{syn}-V_{nt}$) under ^{15}N-labeled ammonia infusion in the rat brain. Moreover, we performed a direct *in vivo* absolute quantification of total Gln, [5-^{15}N]Gln and [2-^{15}N]Glu + Gln in the same experiment.

Materials and methods

Animal Preparation

In vivo ^{15}N and ^{1}H MRS experiments were performed on male Sprague-Dawley rats (six animals, 300 to 350 g), which were fasted overnight (12 hours) with free access to water before the experiment. Rats were anesthetized using isoflurane (Attane, Minrad, NY, USA), intubated and mechanically ventilated (2% isoflurane in O_2 gas). Two femoral veins were cannulated for infusion of α-chloralose (Fisher Scientific, Pittsburgh, PA, USA) and ^{15}N ammonium chloride (99% enriched, Cambridge Isotopes, Andover, MA, USA), and one cannulated artery allowed regular blood sampling for monitoring blood gases, pH and plasma ammonia and urea levels. After the surgery, anesthesia was switched to α-chloralose given as an 80 mg/kg bolus and continuous infusion at 26.7 mg/kg per hour. Afterwards, the head was fixed in a stereotaxic system (bite bar and a pair of ear bars) and the animal was placed in an in-house-built holder. After giving a bolus (0.25 mmol/320 g of body weight) >1 minute (Kanamori *et al*, 1993), ^{15}N ammonium chloride was then continuously infused at 4.5 mmol/h per kilogram. Arterial blood was sampled every hour to

monitor blood gases (PaO_2, $PaCO_2$) and pH using an AVL Compact 3 blood gas analyzer (Roche Diagnostics GmbH, Mannhein, Germany). Plasma ammonia and urea concentrations were measured using an Analox GM7 analyzer (Analox Instruments, London, UK) and a Reflotron Plus analyzer (Roche Diagnostics GmbH), respectively. Respiration rate and volume were adjusted to maintain pH and blood gases within normal physiological ranges ($pH = 7.41 \pm 0.04$; $PaCO_2 = 40.0 \pm 1.8$ mm Hg, O_2 saturation $> 99.8\%$). In addition, sodium bicarbonate (7%, Sigma-Aldrich, Steinheim, Germany) diluted in Dulbecco's Phosphate Buffered Saline (dPBS, Sigma-Aldrich, 70% solution) was infused continuously at an adjustable rate to maintain arterial pH in the normal physiological range. The total amount of blood draw from each animal was $< 10\%$ of the total blood volume of each rat. During the MRS experiments, respiration rate, heart rate, and blood pressure were monitored by a small-animal monitor system (SA Instruments, New York, NY, USA). Body temperature was measured with a rectal thermosensor and maintained at $38.0 \pm 0.5^{\circ}C$ by warm water circulation.

All animal experiments were conducted according to federal and local ethical guidelines and the protocols were approved by the local regulatory body of the Canton Vaud, Switzerland (Service de la consommation et des affaires vétérinaires, Affaires vétérinaires, Canton de Vaud, Suisse).

Magnetic Resonance Spectroscopy Measurements

All ^1H and ^{15}N MRS data were acquired interleaved on a Varian Direct Drive (Palo Alto, CA, USA) console interfaced to an actively shielded 9.4 T magnet (Magnex Scientific, Oxford, UK) with a 31-cm horizontal bore. The magnet was equipped with 12 cm inner-diameter actively shielded gradient sets giving a maximum gradient of 400 mT/m in 120 μs. A home-built 14 mm-diameter ^1H quadrature surface coil combined with a single 5-loop 10 mm ^{15}N coil was used as transceiver. The static field homogeneity was adjusted using first- and second-order shims using an echo-planar version of FASTMAP (Gruetter and Tkac, 2000). Localizer images were obtained in the coronal planes using a multislice fast spin echo protocol with echo time (TE)/repetition time (TR) = 60/5,000 ms, a slice thickness of 1 mm and an in-plane resolution of 94 μm.

^1H spectra were obtained using the ultra-short TE (TE/TR = 2.8/4,000 ms, 4,096 complex data points, SW (spectral width) = 7 kHz, 160 averages) SPin ECho, full Intensity Acquired Localized technique (SPECIAL) (Mlynarik *et al*, 2006, 2008). The voxel of interest (VOI) for ^1H MRS was placed in the center of the brain ($5 \times 7 \times 7$ mm^3). The reproducibility of the voxel placement was based on anatomical landmarks using the localizer images. After first- and second-order shimming, the typical linewidth of water resonance at TE = 2.8 ms was 16 Hz. The water signal was suppressed by a series of seven 25 ms asymmetric variable power radio frequency (RF) pulses with optimized relaxation delays, i.e., VAPOR (Tkac *et al*, 1999). The water suppression pulses were interleaved with three modules of outer volume saturation (OVS) as described previously (Tkac *et al*, 1999). To compensate for the magnetic field drift, spectra were collected in blocks of 16 averages, which were stored separately in the memory and corrected for the relative shift in frequency and potential variations in phase before summation.

^{15}N spectra were acquired using a new pulse sequence based on the previously published Single-shot Inversion Recovery based Non-Echo (SIRENE) sequence (Choi *et al*, 2000). Briefly, in the conventional SIRENE sequence adiabatic pulses (HS8 modulation) are applied to invert the Z magnetization in two x-slices adjacent to the VOI. Then, the magnetization in these two slices follows an inversion recovery trajectory and is minimized by adjusting the inversion time. Residual magnetization outside the VOI was further suppressed by using six OVS pulses applied with a nominal 90° flip angle. The thickness of the upper and lower saturated y-slices was different to adapt the geometry of the rat head. An adiabatic half passage (AHP) pulse was then applied for excitation. In addition, bilevel WALTZ-16 was applied on the ^1H channel for Nuclear Overhauser Effect (NOE) and decoupling during acquisition. Due to the large chemical shift difference between [5-^{15}N]Gln and [2-^{15}N]Glu + Gln ($\sim$70 p.p.m.) in ^{15}N spectra, when using the conventional sequence with the carrier frequency placed on the [5-^{15}N]Gln, the second signal of interest ([2-^{15}N]Glu + Gln) was only partially excited by the AHP RF pulse. Consequently, conventional SIRENE sequence was modified in our study for ^{15}N nuclei by adding a second AHP RF pulse. The two ^{15}N signals of interest were acquired separately in an interleaved mode using two adiabatic excitation pulses with opposite frequency modulations. Figure 1A shows the evolution of the Z magnetization after the first AHP RF pulse with the carrier frequency placed on the [5-^{15}N]Gln. As can be seen,

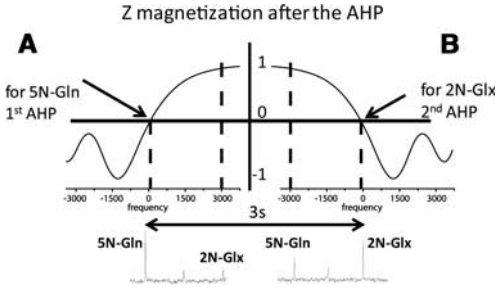

Figure 1 Description of the Z magnetization after the two AHP RF pulses with opposite frequency modulations used interleaved in the new sequence. (**A**) The evolution of the Z magnetization after the first AHP RF pulse with the carrier frequency placed on the [5-^{15}N]Gln. As can be seen, after the AHP RF pulse, [5-^{15}N]Gln was fully excited (no longitudinal magnetization left), but the reduction of the Z magnetization of [2-^{15}N]Glu + Gln was $< 10\%$; (**B**) After 3 seconds, the second AHP RF pulse was applied with the carrier frequency on [2-^{15}N]Glu + Gln and flipped the magnetization of [2-^{15}N]Glu + Gln into the transverse plane, whereas the Z magnetization of [5-^{15}N]Gln was only slightly reduced by this pulse. [5-^{15}N]Gln and [2-^{15}N]Gln + Glu correspond to 5N Gln and 2N Glx in the Figure, respectively. AHP, adiabatic half passage; RF, radio frequency.

after the AHP RF pulse, [5-^{15}N]Gln was fully excited (no longitudinal magnetization left), but the reduction of the Z magnetization of [2-^{15}N]Glu + Gln was $<10\%$. After 3 seconds, the second AHP RF pulse was applied with the carrier frequency on [2-^{15}N]Glu + Gln (Figure 1B). Similarly, the second AHP RF pulse flipped the magnetization of [2-^{15}N]Glu + Gln into the transverse plane, whereas the Z magnetization of [5-^{15}N]Gln was only slightly reduced by this pulse. This interleaved excitation scheme allows to selectively excite the two resonances of interest in the same effective TR. In addition, in our new sequence the adiabatic pulses (HS8 modulation) used to invert the Z magnetization in two x-slices adjacent to the VOI were eliminated; and consequently, the localization was performed by using only the OVS modules. Radio frequency power for excitation, NOE, and decoupling was carefully calibrated using a small sphere (3 mm diameter) containing 99% ^{15}N-enriched glycine (Gly, Cambridge Isotopes) placed at the center of the ^{15}N linear coil as an external reference as described previously (Gruetter *et al*, 1994, 2003). These calibrations were used to establish minimal power necessary for decoupling. Unlocalized ^{15}N spectra were acquired in the first hours of infusion (256 scans, TR = 6 seconds), followed by a localized spectrum (VOI = $5 \times 7 \times 7$ mm^3, 256 scans) used for quantification. The robustness of localization was verified from the absence of the Gly signal in the *in vivo* spectra.

^{15}N-enriched compounds are characterized by a relative long T_1 relaxation time (longitudinal relaxation time). To optimize the TR in the ^{15}N experiments, the *in vitro* T_1 relaxation time of [2-^{15}N]Glu was measured using an adiabatic inversion recovery experiment. The inversion time was varied in the range from 0.1 to 20 seconds. To minimize effects of partial saturation, spectra acquired with different inversion time were collected with the same relaxation delay. The T_1 relaxation curves were fitted with nonweighted two-parameter single exponential functions based on the Levenberg-Marquardt algorithm, fitting M(0) and T_1. For each fit, the correlation coefficients reflecting the quality of the least squares fit versus the original data were computed. A typical standard error of the fitted T_1 was $\sim 5\%$. The *in vitro* T_1 relaxation time of [2-^{15}N]Glu was 4.0 ± 0.3 seconds.

Brain Extraction and *In Vitro* Nuclear Magnetic Resonance Spectroscopy

At the end of each MRS experiment, the animals were killed by focused microwave irradiation within 2 seconds (4 kW, Gerling Applied Engineering, Modesto, CA, USA), which inactivates brain enzymes before extraction (Morgenthaler *et al*, 2006). The dissected brain was immediately frozen in liquid nitrogen and then stored at -80°C until extraction. The frozen brain was powdered in liquid nitrogen with a mortar and pestle and the water-soluble metabolites were extracted with 0.9 mol/L perchloric acid, as previously described (Duarte *et al*, 2007). After vigorous mixing, the preparation was centrifuged at 21,000 *g* for 15 minutes at 4°C. The supernatant was then neutralized with potassium hydroxide (KOH), filtered (Ultrafree-CL filters; Millipore Corporation, Bedford, MA, USA) to remove high molecular weight molecules and dried in a concentrator (SpeedVac Concentrator DNA 120; Thermo Electron Corporation, Milford, MA, USA, PLACE). Afterwards, extracts were resuspended in 500 μL D_2O (99.9% atom D, Sigma-Aldrich, Steinheim, Germany). The pD of the solution was adjusted to ~ 9 to resolve the [2-^{15}N]Gln peak from the [2-^{15}N]Glu peak in high-resolution ^{15}N spectra. The brain extract measurements were performed on a 600-MHz vertical-bore DMX-600 spectrometer (Bruker, Fallanden, Switzerland). One-dimensional pulse-and-acquire ^{15}N spectra were measured with NOE, under fully relaxed conditions (TR = 100 seconds) and with ^{1}H decoupling to measure the [2-^{15}N]Gln and [2-^{15}N]Glu peaks and the corresponding fractional enrichment (FE) ratio (([2-^{15}N]Gln)FE/([2-^{15}N]Glu)FE).

Ammonia concentration in the brain extracts was measured with the Analox GM7 Analyzer as described above for plasma samples.

Spectra Quantification

^{1}H spectra were quantified using LCModel (http://s-provencher.com/pages/lcmodel.shtml) combined with a quantum mechanics simulated basis-set of metabolites based on the density-matrix formalism (Mulkern and Bowers, 1994), using published values of J-coupling constants and chemical shifts (Govindaraju *et al*, 2000), and containing the spectrum of macromolecules measured *in vivo* as described previously (Mlynarik *et al*, 2008; Pfeuffer *et al*, 1999). Absolute quantification was based on the water signal as an internal reference. The Cramér-Rao lower bounds were used as reliability measure of the metabolite concentration estimates.

In vivo and *in vitro* ^{15}N spectra were analyzed using the jMrui software (http://www.mrui.uab.es/mrui/). The signals were fitted using AMARES (Advanced Method for Accurate, Robust, and Efficient Spectral fitting) (Vanhamme *et al*, 1997). For each *in vivo* signal, two Lorentzian spectral components were selected to fit the major contributions of the metabolites ([5-^{15}N]Gln and [2-^{15}N]Gln + Glu), the zero-order phase was estimated and the first-order phase was fixed to zero. The precision of the amplitude estimates was assessed using the Cramér-Rao lower bounds. Absolute quantification was performed using an external reference method described previously for ^{13}C data (Gruetter *et al*, 2003). Briefly, the amplitudes of the localized *in vivo* signals were compared with those obtained under identical experimental conditions from a phantom solution containing ^{15}N uniformly labeled glutamine and glutamate. The effect of variable coil loading on sensitivity was assessed by measuring *in vivo* and in the phantom the signal of the sphere placed at the center of the ^{15}N coil containing an aqueous solution of ^{15}N-labeled Gly. Both measurements of coil loading effects on sensitivity were within 10% to 15% of each other. The NOE and T_1 effects were corrected *in vivo* and *in vitro* by performing each time two different acquisitions: one performed with NOE using the parameters

of the *in vivo* experiment and the second using fully relaxed conditions in absence of NOE (Gruetter *et al*, 1994, 2003).

Metabolic Modeling

The neuroglial two-compartment metabolic model used in the present study is shown in Figure 2. Ammonia ($NH_3 + NH_4^+$) passes the blood–brain barrier and enters glial cells at a rate V_{in}. In astrocytes, ammonia and glutamate are converted to glutamine through GS, thereby labeling the Gln at the position 5N (Figure 2A). Gln is released by the astrocytes and transported into the neurons where it is converted to glutamate by glutaminase, which completes the glutamate–glutamine cycle (Figure 2A). For the labeling of [2-^{15}N]Glu + Gln (Figure 2B), ammonia is incorporated in glial glutamate through GDH, then glutamate is converted to glutamine by GS. Glutamine is transported into neurons and converted to glutamate by neuronal glutaminase. Since most ammonia is detoxified by the GS reaction (Du Ruisseau *et al*, 1957), which is restricted to astrocytes (Martinez-Hernandez *et al*, 1977; Norenberg and Martinez-Hernandez, 1979), and little by GDH (Cooper and Plum, 1987), in the present study we assumed that the astrocyte rather than the neuron is uniquely responsible for ammonia detoxification in the brain.

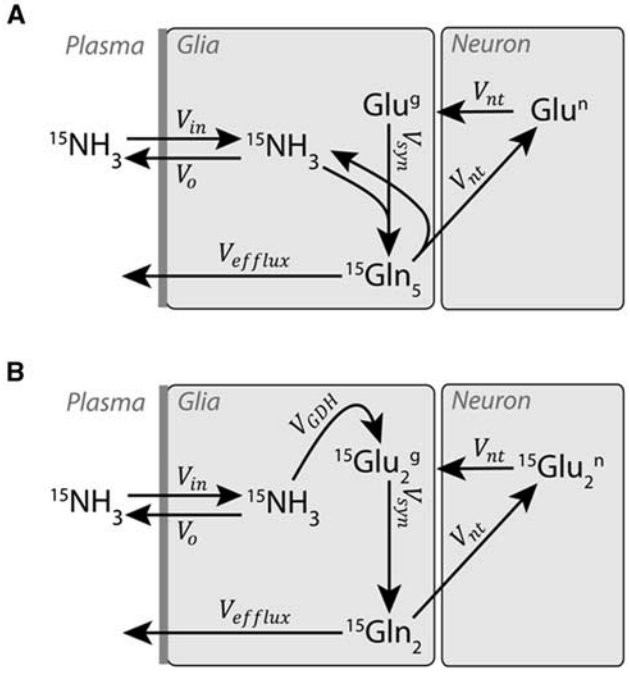

Figure 2 Neuroglial two-compartment metabolic model: (**A**) for [5-^{15}N]Gln: ammonia (NH3 + NH4 +) passes the blood–brain barrier (BBB) and enters glial cells at a rate V_{in}. In astrocytes, ammonia and glutamate are converted to glutamine through glutamine synthetase, thereby labeling the Gln at the position 5N. Gln is released by the astrocytes and transported into the neurons where it is converted to glutamate by glutaminase, which completes the glutamate-glutamine cycle; (**B**) for [2-^{15}N]Gln + Glu: ammonia is incorporated in glutamate through glutamate dehydrogenase, then glutamate is converted to glutamine by glutamine synthetase. Glutamine is transported into neurons and converted to glutamate by neuronal glutaminase. Glial glutaminase was neglected.

In neurons, the exchange of ^{15}N from glutamate in interaction with the tricarboxylic acid cycle happens through transamination reactions, while GDH is essentially taking place in the astrocytes (Aoki *et al*, 1987; Zaganas *et al*, 2001). We modeled the exchange of ^{15}N from the position 2 of neuronal glutamate to the position 2 of aspartate through transamination, assuming a neuronal aspartate pool of 2 μmol/g, as measured by ^{1}H NMR spectroscopy and in agreement with previous reports (Kunz *et al*, 2010; Xin *et al*, 2010). This interaction has the role of a transient dilution of the neuronal [2-^{15}N]Glu pool. We further varied the exchange flux V_x between glutamate and the neuronal tricarboxylic acid cycle through transamination from 0 to 1 μmol/g per minute, which represents a typical range for this chemical exchange in the anesthetized rat brain (Duarte *et al*, 2011). Varying V_x in this range did not affect the labeling curves of [2-^{15}N]Glx significantly and had very low impact on the other determined metabolic fluxes. The model was therefore simplified and the exchange with the neuronal tricarboxylic acid cycle was neglected. We failed to observe any other amino acids to become enriched. A substantial enrichment of aspartate that occurs at ~2 mmol/L (almost exclusively in neurons) would be observable in the ^{15}N spectra.

The time courses of total Gln measured by ^{1}H MRS, [5-^{15}N]Gln, and [2-^{15}N]Glu + Gln were used as experimental data to which the model was fitted as follows. The differential equations derived for [Gln], [5-^{15}N]Gln, and [2-^{15}N]Glu + Gln (see Appendix) were fitted simultaneously using SAAM II environment (The SAAM Institute, Seattle, WA, USA). Since no direct measurement of the dynamic labeling of brain ammonia was possible, V_{in} was assumed 0.23 μmol/g per minute (Cooper *et al*, 1979; Cooper and Plum, 1987; Shen *et al*, 1998). In addition, we assumed a negligible efflux from the Gln pool compared with V_{syn} (Kanamori and Ross, 1993; Kanamori *et al*, 1996; Shen *et al*, 1998). For the fit of [2-^{15}N]Glu + Gln, we assumed that V_{GDH} was mainly in the glial compartment. This assumption was verified by measuring the FE ratio (([2-^{15}N]Gln)FE/([2-^{15}NGlu])FE) in high-resolution ^{15}N brain extract spectra at a pH of ~9. The time evolution of the total Gln, [5-^{15}N]Gln, and [2-^{15}N]Glu + Gln was fitted simultaneously. The linear fit of the time evolution of the total Gln provided a measure of the net glutamine accumulation ($V_{syn} - V_{nt}$) as well as the initial Gln concentration (Gln(0)). In addition, from the fit of the time evolution of [5-^{15}N]Gln we obtained V_{syn} and from these two fluxes ($V_{syn} - V_{nt}$ and V_{syn}) the neurotransmission rate (V_{nt}) was calculated. Finally, using our model the fit of [2-^{15}N]Glu + Gln enabled the measurement of V_{GDH} (see Appendix, equations (18), (19) and (23)). Results were generally presented as mean ± s.d. ($n = 6$).

In addition, using the values obtained for the different fluxes, the FEs of [2-^{15}N]Glu and [2-^{15}N]Gln were simulated for the end of the experiment and their ratio was compared with the high-resolution NMR measurements obtained on brain extracts.

Results

During the *in vivo* experiments, the physiological variables were maintained within normal physiology (pH = 7.41 ± 0.04; $PaCO_2$ = 40.0 ± 1.8 mm Hg, O_2 saturation > 99.8%). The plasma ammonia concentration increased from 0.08 ± 0.02 to 0.95 ± 0.08 mmol/L and remained approximately constant during the experiment. Plasma urea concentration was 7.6 ± 0.8 mmol/L before the ammonium chloride infusion, increased linearly on infusion of ammonium cloride and reached a final concentration of 29.9 ± 10.8 mmol/L. The brain ammonia concentration measured at the end of each experiment in brain extracts was 3.8 ± 0.8 μmol/g in agreement with previous measurements (Kanamori *et al*, 1993, 1996; Kanamori and Ross, 1993). Because ammonia diffuses across the blood–brain barrier mainly as neutral NH_3 and brain pH (7.1) is lower than the blood pH (7.4), brain ammonia level at equilibrium is normally 1.5 to 3 times that of the blood, which is typically maintained under hyperamonemia (Cooper and Plum, 1987). At the end of the infusion period, we determined a brain ammonia/blood ammonia ratio of 3.8 ± 0.8 (mean ± s.d.) that was in the range of previous reports (Cooper and Plum, 1987).

In general, ^{1}H spectra exhibited excellent signal-to-noise ratio allowing easy separation of Gln from Glu. The increase in the total Gln pool at different time points during infusion was thus apparent in the ^{1}H spectra (Figure 3). The total Gln (0) concentration (before starting the infusion) was 2.3 ± 0.4 μmol/g, which increased to 17.7 ± 4.0 μmol/g at the end of the infusion. As can be seen in Figures 3B and 3C, the increase of total Gln started immediately after the infusion and continued to increase linearly over time. The total concentrations of all other metabolites remained within < 10% fluctuation in standard deviation of the mean concentration over the ammonium chloride infusion (i.e., the *N*-acetylaspartate concentration before the ammonium chloride infusion was 7.1 ± 0.5 μmol/g and at the end of infusion was 7.6 ± 0.5 μmol/g). Although lactate concentration was observed to correlate with the total Gln increase (R^2 = 0.90), it never exceeded the physiological range of 2.5 to 3 μmol/g.

To compare the new acquisition sequence with the conventional SIRENE sequence, Figure 4A shows a series of *in vivo* unlocalized ^{15}N spectra acquired in the rat brain during ammonium chloride infusion using the new pulse sequence. It can be observed that the [5-^{15}N]Gln peak (−271 p.p.m.) was detected within 25 minutes, whereas the [2-^{15}N]Gln + Glu peak (−342 p.p.m.) was detected during the second scan (i.e., after 25 minutes of ammonium chloride infusion). With the conventional pulse sequence (Figure 4B), the [5-^{15}N]Gln peak was also visible in the first and all subsequent scans; however, the [2-^{15}N]Gln + Glu peak started to appear only from the fourth scan. Compared with the conventional SIRENE sequence, the new pulse sequence using the

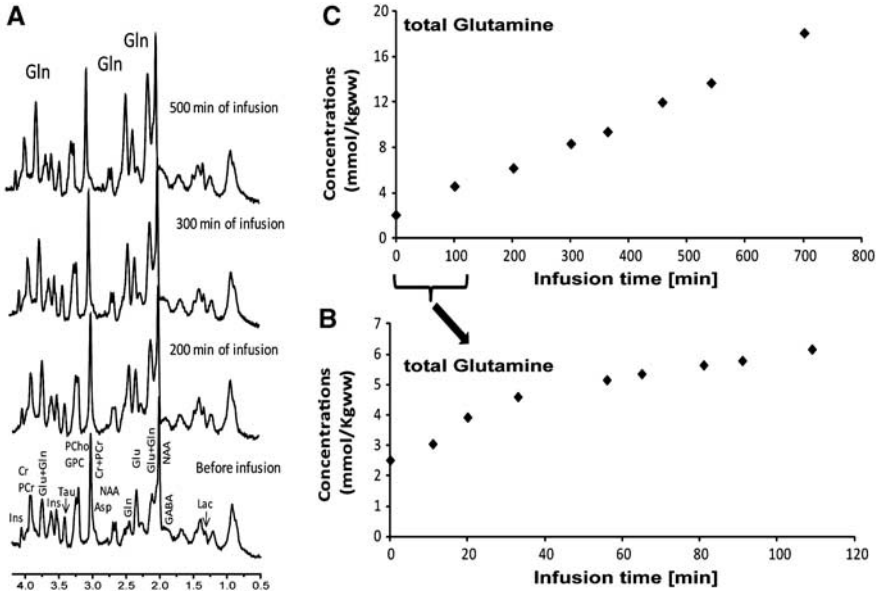

Figure 3 (**A**) Representative *in vivo* ^{1}H spectra acquired at 9.4 T in the rat brain during ammonium chloride infusion (TE/TR = 2.8/4,000 ms, 160 averages, voxel size of 5 × 7 × 7 mm^3); (**B**) Detailed time course of total Gln acquired *in vivo* in the first 2 hours of ^{15}N ammonium chloride infusion; (**C**) The time course of total Gln acquired *in vivo* in one rat more than ~12 hours of ^{15}N ammonium chloride infusion. Phosphocholine (PCho), glycerophosphocholine (GPC), *N*-acetylaspartate (NAA), lactate (Lac), creatine (Cr), phosphocreatine (PCr), taurine (Tau), myo-inositol (Ins), glutamate (Glu), glutamine (Gln), aspartate (Asp), γ-aminobutyrate (GABA). TE, echo time; TR, repitition time.

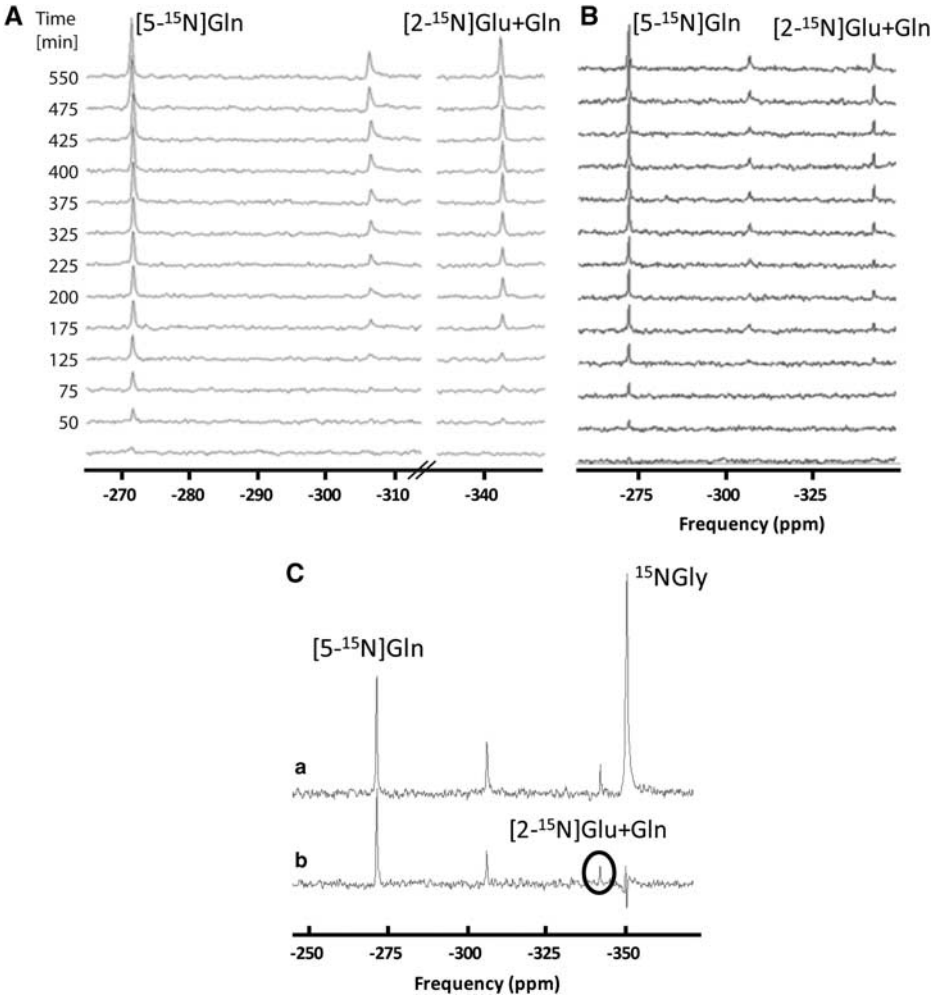

Figure 4 (**A**) A representative series of *in vivo* unlocalized ^{15}N spectra acquired using the new sequence with two AHP RF pulses with opposite frequency modulations at 9.4 T in a rat brain at different time points (two spectra were acquired per TR); (**B**) Representative spectra acquired using the conventional sequence (one spectrum was acquired per TR); (**C**) Localized *in vivo* ^{15}N spectrum acquired in a rat brain (a) during ammonium chloride infusion versus an unlocalized spectrum acquired in the same rat (b) at 25 minutes of interval. The performance of the OVS-based localization is proved by the suppression of the ^{15}N Gly signal, which originates from the sphere placed in the center of the ^{15}N coil. The ^{15}N chemical shifts were referenced to nitromethane. The unmarked resonance in the figures represents the urea signal. AHP, adiabatic half passage; RF, radio frequency; TR, repitition time.

two AHP RF pulses allowed the detection of [2-^{15}N]Gln + Glu peak ~50 minutes earlier due to a better excitation and consequently an increased signal-to-noise ratio.

To assess the performance of the OVS localization technique, Figure 4C shows an example of a localized (a) *in vivo* ^{15}N spectrum versus an unlocalized one (b) acquired at 25 minutes of interval in the same rat during ammonium chloride infusion. As can be seen from the Figure, the performance of the OVS-based localization is proved by the suppression of the ^{15}N Gly signal, which originates from the sphere placed in the center of the ^{15}N coil. In addition, by comparing the two resonances of [5-^{15}N]Gln we can notice that there are very small differences, suggesting that almost the entire [5-^{15}N]Gln signal comes from the brain and not from surrounding tissues.

Using the external reference method described previously for ^{13}C data (Gruetter *et al*, 2003), we were able to perform a direct *in-vivo* absolute quantification for [5-^{15}N]Gln and [2-^{15}N]Gln + Glu. Consequently, at the end of infusion absolute concentrations of [5-^{15}N]Gln and [2-^{15}N]Gln + Glu were 13.3 ± 2.9 and 9.6 ± 3.5 μmol/g, respectively, in accordance with reported *in vitro* brain extracts determinations (biochemical assays or high-resolution NMR; Kanamori *et al*, 1993, 1996; Kanamori and Ross, 1993; Shen *et al*, 1998).

The time courses of total Gln, [5-^{15}N]Gln, and [2-^{15}N]Gln + Glu were highly reproducible in all six rats. The application of the model to the *in vivo* data showed an excellent fit (Figure 5). Using the model presented (Figure 2), we obtained from the ^{1}H data a net Gln accumulation ($V_{syn} - V_{nt}$) of 0.033 ± 0.001 μmol/g per minute (Figure 5A). By

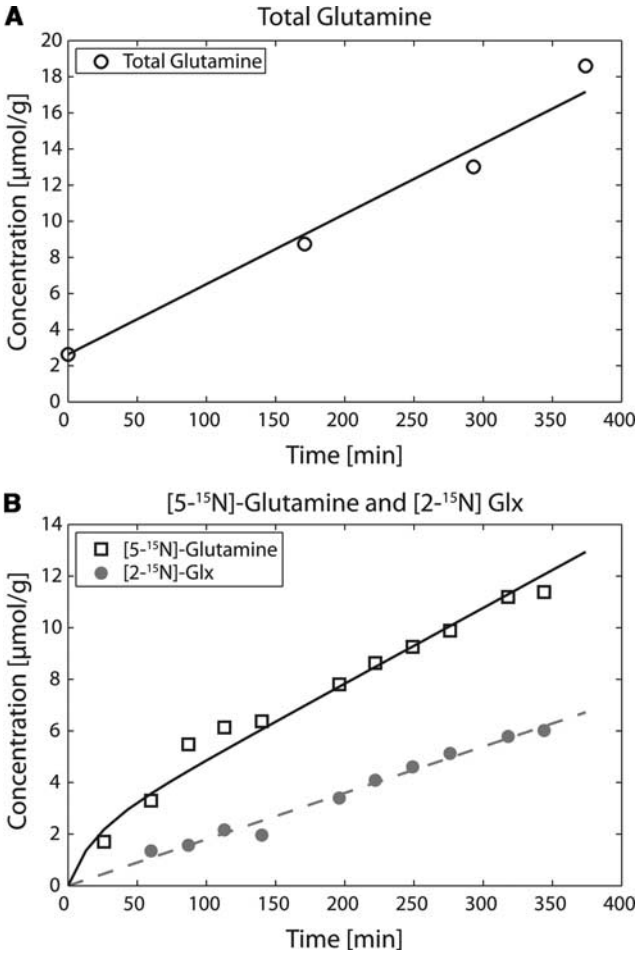

Figure 5 The time courses and corresponding fits of total Gln (**A**), [5-^{15}N]Gln and [2-^{15}N]Gln + Glu (**B**) from one rat (duration of ammonium chloride infusion ~7 hours). [2-^{15}N]Gln + Glu corresponds to [2-^{15}N]Glx in the Figure.

fitting *in vivo* [5-^{15}N]Gln and [2-^{15}N]Glu + Gln time courses (Figure 5B), V_{syn} was 0.30 ± 0.050 μmol/g per minute, V_{GDH} was 0.029 ± 0.002 μmol/g per minute, and the plasma NH_3 FE was $91 \pm 5\%$. Finally, the apparent neurotransmission rate, V_{nt}, was 0.26 ± 0.030 μmol/g per minute.

To determine the predominant cellular localization of GDH, we measured the ratio between the FEs of [2-^{15}N]Gln and [2-^{15}N]Glu in brain extracts. From high-resolution measurements on brain extracts, we calculated ([2-^{15}N]Gln)FE/([2-^{15}N]Glu)FE = 1.48 ± 0.04 which was in agreement with the simulations done for the FEs of [2-^{15}N]Glu and [2-^{15}N]Gln based on the values obtained for the different fluxes.

Discussion

In the present study, we directly and simultaneously measured for the first time V_{syn}, V_{nt}, V_{GDH}, and the net Gln accumulation under ^{15}N-labeled ammonium chloride infusion in the rat brain. This was possible by using a new acquisition strategy: *in vivo* localized ^{15}N MRS interleaved with *in vivo* ^{1}H MRS. In this context, from the modeling point of view this new acquisition strategy required fewer assumptions to determine metabolic rates.

By acquiring *in vivo* ^{1}H spectra, we followed the total Gln accumulation during ammonium chloride infusion. Unlike to previous studies, we directly measured for the first time the net Gln accumulation without any assumptions. Previous measurements of net Gln accumulation (i.e., *de-novo* glutamine synthesis; Shen *et al*, 1998) assumed that the increase of glutamine pool size during hyperammonemia is attributed to increased pyruvate carboxylase and GDH activities. Moreover, these studies assumed that pyruvate carboxylase is equal to GDH under hyperammonemia and that together these fluxes account for the net transport of ammonia.

In addition to the acquisition of *in vivo* ^{1}H spectra, we now simultaneously measured, for the first time, *in vivo* [5-^{15}N]Gln and [2-^{15}N]Gln + Glu time courses during infusion of ^{15}N-enriched ammonium chloride. The new ^{15}N pulse sequence proposed in the present study, which uses the two AHP RF pulses, allowed the detection of [2-^{15}N]Gln + Glu peak ~50 minutes earlier compared with the conventional SIRENE sequence, due to a better excitation and consequently an increased signal-to-noise ratio. Moreover, by acquiring localized ^{15}N spectra and by using the external reference method, we performed a direct *in vivo* absolute quantification for [5-^{15}N]Gln and [2-^{15}N]Gln + Glu. Finally, we directly quantified total Gln, [5-^{15}N]Gln, and [2-^{15}N]Glu + Gln in the same experiment *in vivo* without the need of *in vitro* brain extracts.

The linear and continuous increase of total Gln during the period of ammonium chloride infusion observed in our *in vivo* ^{1}H MRS data implies increased anaplerosis (Berl *et al*, 1962; Shen *et al*, 1998; Zwingmann, 2007), which appears to be coupled to the ammonia detoxification pathway. As can be seen in Figures 3B and 3C, the increase of total Gln started immediately after the infusion and was linear over the infusion time, in contrast to previous studies (Rothman *et al*, 1999; Shen *et al*, 1998), suggesting that no delay in Gln accumulation was observed. The total Gln concentration measured at the end of the infusion is comparable to previous studies based on *in vitro* brain extract determinations (Kanamori *et al*, 1993, 1996; Kanamori and Ross, 1993; Shen *et al*, 1998). Using our metabolic model, Gln(0) (initial total glutamine concentration measured under standard physiological conditions) was also fitted and the obtained value (2.4 ± 0.3 μmol/g) is in agreement with the measured concentration of 2.3 ± 0.4 μmol/g. Contrary to previous studies under ammonia infusion, we continuously quantified the total Gln increase over time, which allowed us to directly measure net Gln accumulation without any assumptions. The obtained $V_{syn} - V_{nt}$ of 0.033 ± 0.001 μmol/g per minute was twofold lower than

the previously reported value under hyperammonemia measured indirectly by extrapolation using ^{15}N MRS (Shen *et al*, 1998). The main source of discrepancy between our study and the previous one may be related to the fact that the previous study required modeling extrapolation to estimate net Gln accumulation.

The pyruvate carboxylation flux measured using ^{13}C MRS under normoammonimic conditions is well known to be high in the conscious rat (Oz *et al*, 2004) and nearly absent under isoelectricity (Choi *et al*, 2002; Sibson *et al*, 1998), whereas under light α-chloralose anesthesia was measured to be 0.07 μmol/g per minute (Duarte *et al*, 2011). In the present study, the measurement of the pyruvate carboxylation flux gave a lower limit, which is likely to be higher due to pyruvate recycling and glutamine efflux. Consequently, the *de-novo* glutamine synthesis measured in our study under hyperammonemia might be assumed to be equal to the sum of the pyruvate carboxylation flux measured under normoammonimic conditions (Duarte *et al*, 2011) and the net Gln accumulation measured in our study under hyperammonemia, i.e., 0.07 + 0.033 = 0.103 μmol/g per minute. This estimated value under hyperammonemia for the *de-novo* glutamine synthesis is similar to previously reported unidirectional measurements under hyperammonemia using ^{13}C MRS (Sibson *et al*, 2001) and indicated a significant increase in anaplerotic flux during hyperammonemia supporting the hypothesis that the anaplerotic flux is coupled to nitrogen removal from the brain (ammonia detoxification) under hyperammonemia conditions (Berl *et al*, 1962; Sibson *et al*, 2001; Zwingmann, 2007).

The incorporation of ^{15}N of ammonia into [5-^{15}N]Gln gave a V_{syn} of 0.30 ± 0.050 μmol/g per minute, which was higher than previous published data under hyperammonemia ranging from 0.06 to 0.20 μmol/g per minute obtained when using ^{15}N MRS (Kanamori *et al*, 1993, 1996; Kanamori and Ross, 1993; Shen *et al*, 1998) and lower than 0.29 to 0.43 μmol/g per minute (Sibson *et al*, 1997, 2001) obtained when using ^{13}C MRS. As discussed previously, the main source of discrepancy between our study and the previous ones might be related to the increased number of assumptions used for the modeling of the previous studies. Together with V_{syn}, we also fitted the plasma NH_3 FE which was 91 ± 5%, consistent with experimental measurements (Shen *et al*, 1998). The apparent GS rate obtained in the present study under hyperammonemia conditions 0.30 ± 0.050 μmol/g per minute (see Results) was higher than the value of 0.18 μmol/g per minute reported under normoammonimic conditions using ^{13}C MRS (Duarte *et al*, 2011), supporting the role of GS as a detoxification pathway for ammonia in the brain.

From the values of $V_{syn} - V_{nt}$ of 0.033 ± 0.001 μmol/g per minute and V_{syn} of 0.30 ± 0.050 μmol/min per gram, we obtained a V_{nt} of 0.26 ± 0.030 μmol/g per minute. Our results (see Results) indicate that under hyperammonemia conditions the neurotransmission rate represents ~80% of the flux through the GS which is comparable to the values reported previously using ^{15}N MRS or ^{13}C MRS (Shen *et al*, 1998; Sibson *et al*, 1997, 2001). Since in the present study, we are assuming a negligible efflux from the Gln pool compared with V_{syn} based on previous reports (Kanamori and Ross, 1993; Kanamori *et al*, 1996; Shen *et al*, 1998), the obtained neurotransmission rate V_{nt} represents an upper limit. By considering a Gln efflux of 0.07 μmol/g per minute (Duarte *et al*, 2011), we obtain a lower limit for V_{nt} of 0.19 μmol/g per minute which is similar with the value reported under normoammonimic conditions using ^{13}C MRS (Duarte *et al*, 2011).

Although [2-^{15}N] Glu and [2-^{15}N] Gln cannot be separated in ^{15}N spectra *in vivo*, the application of the model (Figure 2B; equations (18), (19) and (23) from Appendix) provided a V_{GDH} with a high precision. Consequently, the incorporation of ^{15}N into [2-^{15}N]Gln + Glu alone, provided a V_{GDH} of 0.029 ± 0.002 μmol/g per minute, where V_{syn} and V_{nt} needed to model the exchange between [2-^{15}N] Glu and [2-^{15}N] Gln were obtained from the simultaneous fit of the position 5N and total Gln. To maintain a constant Glu concentration with increasing Gln, glutamate needs to be synthesized from tricarboxylic acid intermediates. To determine the predominant cellular localization of GDH, we performed high-resolution measurements on brain extracts and consequently measured the ratio between the FEs of [2-^{15}N]Glu and [2-^{15}N]Gln (see Results). From these measurements, we obtained ([2-^{15}N]Gln)FE > ([[2-^{15}N]Glu)FE which showed that net glutamate synthesis results from higher GDH activity in the glial compartment. Note that previous studies assumed that this replenishment takes place primarily in the glial compartment in hyperammonemic conditions (Shen *et al*, 1998). The high glial GDH flux obtained in our study is in agreement with higher specific activity in astrocytes relative to neurons (Schmitt and Kugler, 1999; Zaganas *et al*, 2001). In the presented model, a unidirectional flux was assumed for GDH in the astrocytes. When including a reversible flux for the GDH reaction, the reversible component of GDH was always converging to zero in the fitting process. In addition, our results also showed that under hyperammonemia $V_{GDH} \approx (V_{syn} - V_{nt})$, meaning that the rate of breakdown of Glu to glial 2-oxoglutarate was negligible. To our knowledge, there was only one previous study which measured V_{GDH} under ^{15}N ammonia infusion (Kanamori and Ross, 1995) reporting a V_{GDH} value of 0.018 to 0.020 μmol/min per gram for an infusion rate of 3.3 mmol/kg per hour, which is consistent with our results considering that our infusion rate was higher (4.5 mmol/kg per hour) and thus likely to stimulate glutamine synthesis.

The incorporation of ^{15}N of ammonia takes place mainly into [5-^{15}N]Gln through V_{syn} and into

[2-^{15}N]Glu + Gln through V_{GDH}. Since V_{GDH} obtained in our study represents only 10% from the obtained V_{syn}, it supports the concept of GS as a major detoxification pathway for ammonia in the brain.

We conclude that it is feasible to combine localized *in vivo* ^{15}N with ^{1}H MRS and with an appropriate mathematical model to directly, simultaneously and reliably detect for the first time along with V_{syn}, the net glutamine accumulation, V_{nt} and V_{GDH} under ammonia infusion in the *in vivo* rat brain. From the modeling point of view, this new acquisition strategy required fewer assumptions to determine metabolic rates. In addition, this new strategy allowed a robust absolute quantification of total Gln, [5-^{15}N]Gln and [2-^{15}N]Gln + Glu in the same experiment. Our results showed an increase of GS and net glutamine accumulation under hyperammonemia, supporting the concept of their implication in cerebral ammonia detoxification. In addition, under hyperammonemia conditions the neurotransmission rate represents $\sim$80% of the flux through the GS. The higher ([2-^{15}N]Gln)FE compared with ([[2-^{15}N]Glu)FE showed that net glutamate synthesis results from higher GDH activity in the glial compartment. Our results also showed that under hyperammonemia the rate of breakdown of Glu to glial 2-oxoglutarate was negligible because $V_{GDH} \approx (V_{syn} - V_{nt})$. Finally, the role of GS as an important detoxification pathway for ammonia in the brain was also supported by the fact that, in our study, the obtained V_{GDH} was smaller than V_{syn}.

Acknowledgements

The authors thank Dr PR Vasos (Laboratory for Biomolecular Magnetic Resonance, Ecole Polytechnique Federale de Lausanne, Lausanne, Switzerland) for this help with the acquisition of high resolution data and Dr N Kunz (Laboratory for Functional and Metabolic Imaging (LIFMET), Center for Biomedical Imaging (CIBM), Ecole Polytechnique Fédérale de Lausanne (EPFL), Lausanne, Switzerland) for providing the Matlab routines for preprocessing of ^{1}H MRS data.

Disclosure/conflict of interest

The authors declare no coflict of interest.

References

Aoki C, Milner TA, Sheu KF, Blass JP, Pickel VM (1987) Regional distribution of astrocytes with intense immunoreactivity for glutamate dehydrogenase in rat brain: implications for neuron-glia interactions in glutamate transmission. *J Neurosci* 7:2214–31

Berl S, Nicklas WJ, Clarke DD (1968) Compartmentation of glutamic acid metabolism in brain slices. *J Neurochem* 15:131–40

Berl S, Takagaki G, Clarke DD, Waelsch H (1962) Metabolic compartments *in vivo*. Ammonia and glutamic acid metabolism in brain and liver. *J Biol Chem* 237:2562–9

Butterworth RF, Girard G, Giguere JF (1988) Regional differences in the capacity for ammonia removal by brain following portocaval anastomosis. *J Neurochem* 51:486–90

Choi IY, Lei H, Gruetter R (2002) Effect of deep pentobarbital anesthesia on neurotransmitter metabolism *in vivo*: on the correlation of total glucose consumption with glutamatergic action. *J Cereb Blood Flow Metab* 22:1343–51

Choi IY, Tkac I, Gruetter R (2000) Single-shot, three-dimensional 'non-echo' localization method for *in vivo* NMR spectroscopy. *Magn Reson Med* 44:387–94

Clarke DD, Nicklas WJ, Berl S (1970) Tricarboxylic acid-cycle metabolism in brain. Effect of fluoroacetate and fluorocitrate on the labelling of glutamate, aspartate, glutamine and gamma-aminobutyrate. *Biochem J* 120:345–51

Cooper AJ, McDonald JM, Gelbard AS, Gledhill RF, Duffy TE (1979) The metabolic fate of 13N-labeled ammonia in rat brain. *J Biol Chem* 254:4982–92

Cooper AJ, Plum F (1987) Biochemistry and physiology of brain ammonia. *Physiol Rev* 67:440–519

Du Ruisseau JP, Greenstein JP, Winitz M, Birnbaum SM (1957) Studies on the metabolism of amino acids and related compounds *in vivo*. VI. Free amino acid levels in the tissues of rats protected against ammonia toxicity. *Arch Biochem Biophys* 68:161–71

Duarte JMN, Cunha RA, Carvalho RA (2007) Different metabolism of glutamatergic and GABAergic compartments in superfused hippocampal slices characterized by nuclear magnetic resonance spectroscopy. *Neuroscience* 144:1305–13

Duarte JMN, Lanz B, Gruetter R (2011) Compartmentalised cerebral metabolism of [1,6-13C]glucose determined by *in vivo* 13C NMR spectroscopy at 14.1 T. *Front Neuroenergetics* 3:3

Erecinska M, Silver IA (1990) Metabolism and role of glutamate in mammalian brain. *Prog Neurobiol* 35:245–96

Fitzpatrick SM, Hetherington HP, Behar KL, Shulman RG (1989) Effects of acute hyperammonemia on cerebral amino acid metabolism and pHi *in vivo*, measured by 1H and 31P nuclear magnetic resonance. *J Neurochem* 52:741–9

Govindaraju V, Young K, Maudsley AA (2000) Proton NMR chemical shifts and coupling constants for brain metabolites. *NMR Biomed* 13:129–53

Gruetter R (2004) Principles of the measurment of neuroglial metabolism using *in vivo* 13C NMR spectroscopy. *Adv Mol Cell Biol* 31:409–33

Gruetter R, Adriany G, Choi IY, Henry PG, Lei H, Oz G (2003) Localized *in vivo* 13C NMR spectroscopy of the brain. *NMR Biomed* 16:313–38

Gruetter R, Novotny EJ, Boulware SD, Mason GF, Rothman DL, Shulman GI, Prichard JW, Shulman RG (1994) Localized 13C NMR spectroscopy in the human brain of amino acid labeling from D-[1-13C]glucose. *J Neurochem* 63:1377–85

Gruetter R, Seaquist ER, Ugurbil K (2001) A mathematical model of compartmentalized neurotransmitter metabolism in the human brain. *Am J Physiol Endocrinol Metab* 281:E100–12

Gruetter R, Tkac I (2000) Field mapping without reference scan using asymmetric echo-planar techniques. *Magn Reson Med* 43:319–23

Kanamori K, Parivar F, Ross BD (1993) A 15N NMR study of *in vivo* cerebral glutamine synthesis in hyperammonemic rats. *NMR Biomed* 6:21–6

Kanamori K, Ross BD (1993) 15N n.m.r. measurement of the *in vivo* rate of glutamine synthesis and utilization at steady state in the brain of the hyperammonaemic rat. *Biochem J* 293(Part 2):461–8

Kanamori K, Ross BD (1995) Steady-state *in vivo* glutamate dehydrogenase activity in rat brain measured by 15N NMR. *J Biol Chem* 270:24805–9

Kanamori K, Ross BD, Chung JC, Kuo EL (1996) Severity of hyperammonemic encephalopathy correlates with brain ammonia level and saturation of glutamine synthetase *in vivo*. *J Neurochem* 67:1584–94

Kunz N, Cudalbu C, Mlynarik V, Huppi PS, Sizonenko SV, Gruetter R (2010) Diffusion-weighted spectroscopy: a novel approach to determine macromolecule resonances in short-echo time ^{1}H-MRS. *Magn Reson Med* 64:939–46

Martinez-Hernandez A, Bell KP, Norenberg MD (1977) Glutamine synthetase: glial localization in brain. *Science* 195:1356–8

McKenna MC (2007) The glutamate-glutamine cycle is not stoichiometric: fates of glutamate in brain. *J Neurosci Res* 85:3347–58

Mlynarik V, Cudalbu C, Xin L, Gruetter R (2008) 1H NMR spectroscopy of rat brain *in vivo* at 14.1Tesla: improvements in quantification of the neurochemical profile. *J Magn Reson* 194:163–8

Mlynarik V, Gambarota G, Frenkel H, Gruetter R (2006) Localized short-echo-time proton MR spectroscopy with full signal-intensity acquisition. *Magn Reson Med* 56:965–70

Morgenthaler FD, Koski DM, Kraftsik R, Henry PG, Gruetter R (2006) Biochemical quantification of total brain glycogen concentration in rats under different glycemic states. *Neurochem Int* 48:616–22

Mulkern R, Bowers J (1994) Density matrix calculations of AB spectra from multipulse sequences: quantum mechanics meets *in vivo* spectroscopy. *Concepts Magn Reson* 6:1–23

Norenberg MD, Martinez-Hernandez A (1979) Fine structural localization of glutamine synthetase in astrocytes of rat brain. *Brain Res* 161:303–10

Oz G, Berkich DA, Henry PG, Xu Y, LaNoue K, Hutson SM, Gruetter R (2004) Neuroglial metabolism in the awake rat brain: CO2 fixation increases with brain activity. *J Neurosci* 24:11273–9

Pfeuffer J, Tkac I, Provencher SW, Gruetter R (1999) Toward an *in vivo* neurochemical profile: quantification of 18 metabolites in short-echo-time (1)H NMR spectra of the rat brain. *J Magn Reson* 141:104–20

Rothman DL, Sibson NR, Hyder F, Shen J, Behar KL, Shulman RG (1999) *In vivo* nuclear magnetic resonance spectroscopy studies of the relationship between the glutamate-glutamine neurotransmitter cycle and functional neuroenergetics. *Philos Trans R Soc Lond B Biol Sci* 354:1165–77

Schmitt A, Kugler P (1999) Cellular and regional expression of glutamate dehydrogenase in the rat nervous system: non-radioactive *in situ* hybridization and comparative immunocytochemistry. *Neuroscience* 92:293–308

Shank RP, Aprison MH (1981) Present status and significance of the glutamine cycle in neural tissues. *Life Sci* 28:837–42

Shen J, Sibson NR, Cline G, Behar KL, Rothman DL, Shulman RG (1998) 15N-NMR spectroscopy studies of ammonia transport and glutamine synthesis in the hyperammonemic rat brain. *Dev Neurosci* 20:434–43

Sibson NR, Dhankhar A, Mason GF, Behar KL, Rothman DL, Shulman RG (1997) *In vivo* 13C NMR measurements of cerebral glutamine synthesis as evidence for glutamate-glutamine cycling. *Proc Natl Acad Sci USA* 94:2699–704

Sibson NR, Dhankhar A, Mason GF, Rothman DL, Behar KL, Shulman RG (1998) Stoichiometric coupling of brain glucose metabolism and glutamatergic neuronal activity. *Proc Natl Acad Sci USA* 95:316–21

Sibson NR, Mason GF, Shen J, Cline GW, Herskovits AZ, Wall JE, Behar KL, Rothman DL, Shulman RG (2001) *In vivo* (13)C NMR measurement of neurotransmitter glutamate cycling, anaplerosis and TCA cycle flux in rat brain during. *J Neurochem* 76:975–89

Tkac I, Starcuk Z, Choi IY, Gruetter R (1999) *In vivo* 1H NMR spectroscopy of rat brain at 1 ms echo time. *Magn Reson Med* 41:649–56

Uffmann K, Gruetter R (2007) Mathematical modeling of (13)C label incorporation of the TCA cycle: the concept of composite precursor function. *J Neurosci Res* 85:3304–17

Vanhamme L, van den Boogaart A, Van Huffel S (1997) Improved method for accurate and efficient quantification of MRS data with use of prior knowledge. *J Magn Reson* 129:35–43

Xin L, Gambarota G, Duarte JM, Mlynarik V, Gruetter R (2010) Direct *in vivo* measurement of glycine and the neurochemical profile in the rat medulla oblongata. *NMR Biomed* 23:1097–102

Yudkoff M, Nissim I, Hummeler K, Medow M, Pleasure D (1986) Utilization of [15N]glutamate by cultured astrocytes. *Biochem J* 234:185–92

Zaganas I, Waagepetersen HS, Georgopoulos P, Sonnewald U, Plaitakis A, Schousboe A (2001) Differential expression of glutamate dehydrogenase in cultured neurons and astrocytes from mouse cerebellum and cerebral cortex. *J Neurosci Res* 66:909–13

Zwingmann C (2007) The anaplerotic flux and ammonia detoxification in hepatic encephalopathy. *Metab Brain Dis* 22:235–49

Zwingmann C, Leibfritz D (2003) Regulation of glial metabolism studied by 13C-NMR. *NMR Biomed* 16:370–99

Appendix

Derivation of the Differential Equations for Brain Metabolism During [^{15}N]Ammonia Infusion

(A) Modeling of the Total Glutamine Concentration (^{1}H MRS Measurement)

In the neuroglial two-compartment metabolic model (Figure 2), metabolic steady-state was assumed for the metabolic fluxes, i.e., the fluxes V are assumed to be constant throughout the duration of the experiment.

Applying mass balance, we obtained:

$$\frac{d[Glu]}{dt} = \frac{d[Glu^n]}{dt} + \frac{d[Glu^g]}{dt} = V_{nt} - V_{nt} + V_{nt} + V_g - V_{syn} = V_{nt} + V_g - V_{syn} \quad (1)$$

$$\frac{d[Gln]}{dt} = V_{syn} - V_{nt} - V_{efflux} \quad (2)$$

However, as confirmed by the ^{1}H NMR spectra, not all the concentrations of the metabolites of interest were constant over time in conditions of hyperammonemia. The concentration of glutamate was stable, while the concentration of glutamine increased linearly over time. The constant glutamate concentration gave the following relationship between the fluxes:

$$\frac{d[Glu]}{dt} = 0 \Rightarrow V_{syn} = V_{nt} + V_g \quad (3)$$

Assuming constant metabolic fluxes, the differential equation for the total glutamine concentration can be solved:

$$[Gln](t) = [Gln](0) + (V_{syn} - V_{nt} - V_{efflux})t \quad (4)$$

It was reported (Kanamori and Ross, 1993; Kanamori *et al*, 1996; Shen *et al*, 1998) that V_{efflux} was small compared with V_{syn} and equation 4 was therefore simplified to:

$$[Gln](t) = [Gln](0) + (V_{syn} - V_{nt})t \quad (5)$$

Where [Gln](0) is the initial total glutamine concentration measured under standard physiological conditions, i.e., before starting the infusion of ammonia.

(B) Modeling of the [5-^{15}N] Glutamine Concentration

We assumed metabolic steady-state conditions for the fluxes and involved chemical pools, except for glutamine. The labeling equation for brain ammonia was given by:

$$\frac{d[NH_3]_{brain}}{dt} = V_{in} + V_{nt} - (V_o + V_{syn} + V_{GDH}) = 0 \quad (6)$$

$$\Rightarrow V_o = V_{in} + V_{nt} - V_{syn} - V_{GDH}$$

$$\frac{d^{15}NH_{3_{brain}}}{dt} = V_{in}\frac{^{15}NH_{3_{plasma}}}{[NH_3]_{plasma}} + V_{nt}\frac{[5-^{15}N]Gln}{[Gln]} - (V_o + V_{syn} + V_{GDH})\frac{^{15}NH_{3_{brain}}}{[NH_3]_{brain}} \quad (7)$$

The isotopic enrichment of ammonia in plasma (FE_{plasma}) was assumed to be constant during the infusion period, which was valid and consistent with relatively low ammonia levels before infusion (0.08 ± 0.02 mmol). Using the result of equation (6), equation (7) can be rewritten:

$$\frac{d^{15}NH_{3_{brain}}}{dt} = V_{in}\,FE_{plasma} + V_{nt}\frac{[5-^{15}N]Gln}{[Gln]} - (V_{in} + V_{nt})\frac{^{15}NH_{3_{brain}}}{[NH_3]_{brain}} \quad (8)$$

The labeling of [5-^{15}N] glutamine was thus given by:

$$\frac{d[5-^{15}N]Gln}{dt} = V_{syn}\frac{^{15}NH_{3_{brain}}}{[NH_3]_{brain}} - V_{nt}\frac{[5-^{15}N]Gln}{[Gln]} \quad (9)$$

The first term on the right of equation (9) can be isolated from the labeling equation of brain ammonia (equation (8)). Equation (9) is then rewritten as:

$$\frac{d[5-^{15}N]Gln}{dt} = V_{syn}\left(\frac{V_{in}}{(V_{in}+V_{nt})}FE_{plasma} + \frac{V_{nt}}{(V_{in}+V_{nt})}\frac{[5-^{15}N]Gln}{[Gln]} - \frac{1}{(V_{in}+V_{nt})}\frac{d^{15}NH_{3_{brain}}}{dt}\right) - V_{nt}\frac{[5-^{15}N]Gln}{[Gln]} \quad (10)$$

$$\frac{d[5-^{15}N]Gln}{dt} + \frac{V_{syn}}{(V_{in}+V_{nt})}\frac{d^{15}NH_{3_{brain}}}{dt} = V_{syn}\left(\frac{V_{in}}{(V_{in}+V_{nt})}FE_{plasma} + \frac{V_{nt}}{(V_{in}+V_{nt})}\frac{[5-^{15}N]Gln}{[Gln]}\right) - V_{nt}\frac{[5-^{15}N]Gln}{[Gln]} \quad (11)$$

Changes in $NH_{3\ brain}$ were assumed to be small in comparison with the glutamine pool ('small pool approximation'; Duarte *et al*, 2011; Uffmann and Gruetter, 2007), i.e.:

$$\frac{d[5-^{15}N]Gln}{dt} \gg \frac{d^{15}NH_{3_{brain}}}{dt} \quad (12)$$

Equation (11) is then simplified to:

$$\frac{d[5-^{15}N]Gln}{dt} = \frac{V_{syn}V_{in}}{(V_{in}+V_{nt})}FE_{plasma} + \frac{V_{syn}V_{nt}}{(V_{in}+V_{nt})}\frac{[5-^{15}N]Gln}{[Gln]} - V_{nt}\frac{[5-^{15}N]Gln}{[Gln]} \quad (13)$$

In equation (13), not only the ^{15}N-labeled metabolite concentrations are changing over time, but also [Gln] was increasing, as described in part (A) of this appendix. Using equation (5), equation (13) can be rewritten more explicitly:

$$\frac{d[5-^{15}N]Gln}{dt} = \frac{V_{syn}V_{in}}{(V_{in}+V_{nt})}FE_{plasma} + \frac{V_{syn}V_{nt}}{(V_{in}+V_{nt})}\frac{[5-^{15}N]Gln}{[Gln](0)+(V_{syn}-V_{nt})t} - V_{nt}\frac{[5-^{15}N]Gln}{[Gln](0)+(V_{syn}-V_{nt})t} \quad (14)$$

$$\frac{d[5-^{15}N]Gln}{dt} = \frac{V_{syn}V_{in}}{(V_{in}+V_{nt})}FE_{plasma} - V_{nt}\left[\frac{(V_{in}+V_{nt})-V_{syn}}{(V_{in}+V_{nt})}\right]\frac{[5-^{15}N]Gln}{[Gln](0)+(V_{syn}-V_{nt})t} \quad (15)$$

From the equation (15), the initial slope of the [5-^{15}N]Gln labeling curve can be derived:

$$\lim_{t\to 0}\left(\frac{d[5-^{15}N]Gln}{dt}\right) = \frac{V_{syn}V_{in}}{(V_{in}+V_{nt})}FE_{plasma}, \quad \text{since } [5-^{15}N]Glu(0)=0 \quad (16)$$

(C) Modeling of the [2-^{15}N] Glutamine and Glutamate Concentrations

From the model presented in Figure 2B, the rate of labeling of [2-^{15}N]Glu^{g}, [2-^{15}N]Glu^{n}, [2-^{15}N]Gln was expressed as:

$$\frac{d[2-^{15}N]Glu^{g}}{dt} = V_{GDH}\frac{^{15}NH_{3_{brain}}}{[NH_3]_{brain}} - V_{syn}\frac{[2-^{15}N]Glu^{g}}{[Glu^{g}]} + V_{nt}\frac{[2-^{15}N]Glu^{n}}{[Glu^{n}]} \quad (17)$$

$$\frac{d[2-^{15}N]Glu^{n}}{dt} = V_{nt}\frac{[2-^{15}N]Gln}{[Gln]} - V_{nt}\frac{[2-^{15}N]Glu^{n}}{[Glu^{n}]} \quad (18)$$

$$\frac{d[2-^{15}N]Gln}{dt} = V_{syn}\frac{[2-^{15}N]Glu^{g}}{[Glu^{g}]} - V_{nt}\frac{[2-^{15}N]Gln}{[Gln]} \quad (19)$$

Again, [Gln] is not a constant pool in the case of hyperammonemia and has to be included in the modeling. The 'small pool approximation' (Duarte *et al*, 2011; Uffmann and Gruetter, 2007) was assumed for $^{15}NH_{3\ brain}$. Using equation (8), the isotopic enrichment of brain ammonia can be isolated and injected in equation (17):

$$\frac{d[2-^{15}N]Glu^{g}}{dt} = V_{GDH}\left(\frac{V_{in}}{(V_{in}+V_{nt})}FE_{plasma} + \frac{V_{nt}}{(V_{in}+V_{nt})}\frac{[5-^{15}N]Gln}{[Gln]} \frac{1}{(V_{in}+V_{nt})}\frac{d^{15}NH_{3_{brain}}}{dt}\right) - V_{syn}\frac{[2-^{15}N]Glu^{g}}{[Glu^{g}]} + V_{nt}\frac{[2-^{15}N]Glu^{n}}{[Glu^{n}]} \quad (20)$$

$$\frac{d[2-^{15}N]Glu^{g}}{dt} + V_{GDH}\frac{1}{(V_{in}+V_{nt})}\frac{d^{15}NH_{3_{brain}}}{dt} = V_{GDH}\left(\frac{V_{in}}{(V_{in}+V_{nt})}FE_{plasma} + \frac{V_{nt}}{(V_{in}+V_{nt})}\frac{[5-^{15}N]Gln}{[Gln]}\right) - V_{syn}\frac{[2-^{15}N]Glu^{g}}{[Glu^{g}]} + V_{nt}\frac{[2-^{15}N]Glu^{n}}{[Glu^{n}]} \quad (21)$$

The 'small pool approximation' was given by the following expression:

$$\frac{d[2-^{15}N]Glu^{g}}{dt} \gg \frac{d^{15}NH_{3_{brain}}}{dt} \quad (22)$$

Finally, the labeling equation of glial glutamate (equation (17)) can be directly written in terms of plasma ammonia enrichment as:

$$\frac{d[2-^{15}N]Glu^{g}}{dt} = V_{GDH}\left(\frac{V_{in}}{(V_{in}+V_{nt})}FE_{plasma} + \frac{V_{nt}}{(V_{in}+V_{nt})}\frac{[5-^{15}N]Gln}{[Gln]}\right) - V_{syn}\frac{[2-^{15}N]Glu^{g}}{[Glu^{g}]} + V_{nt}\frac{[2-^{15}N]Glu^{n}}{[Glu^{n}]} \quad (23)$$

Equations (18), (19) and (23) are a set of three coupled differential equations, also coupled to the [5-^{15}N]Gln enrichment. The measured [2-^{15}N]Glu + Gln was then fitted to the sum of the numerical solution of these equations.